Finite Element Modelling of Post-tensioned Timber Beams at Ambient and Fire Conditions

Hailey Quiquero, Entuitive, Toronto, Canada
John Gales ⓘ* and Rwayda Al Hamd, York University, Toronto, Canada
Anthony Abu, University of Canterbury, Christchurch, New Zealand

Abstract. An increased environmental conscientiousness in society and the abundance of timber in Canada has inevitably led to the desire for more timber construction. In order to increase the opportunity for timber products in construction, novel building systems such as post-tensioned (PT) timber have been developed. Limited development on numerical modelling has been done on PT timber systems for the optimization of design for fire performance. In industry, there is need for a modelling software capable of approximating complex timber system behaviours that is accessible to practitioners. This research program serves to evaluate the current capabilities or shortcomings of modelling PT timber in both ambient and fire conditions, and to develop a methodology for analyzing the performance of the system. Several numerical models of PT timber beam tests are developed and validated using general purpose FEM software ABAQUS. This software is a good research tool and the lessons learned may be used to refine an accessible model for practitioners. Various material definitions are compared including isotropic and orthotropic models. The numerical models show highly promising results for demonstrating the loading and failure behaviour of PT timber beams. Material property directionality is paramount, captured best with the use of Hill's Potential Function for non-elastic behaviour. Ambient beam tests are modelled with accurately demonstrated load–deflection behaviour and peak loads are computed to within 5% of experimentally recorded values. For PT timber beam standard fire furnace tests, beam failure times are modelled within 3 min of experimental beam failure times for various fire exposure durations (about 5%), and load–deflection behaviour and failure mechanisms are accurately demonstrated. Thermal gradients align with the recorded thermocouple readings and char depths are computed within 4 mm of the observed layers.

---

* Correspondence should be addressed to: John Gales, E-mail: jgales@yorku.ca

1. Introduction and Background

In recent years the popularity of timber as a commercial building material has greatly increased. Today, the benefits of large-scale massive timber construction include savings in weight, labour, construction time, and carbon footprint compared to other building materials. For example, the construction of Brock Commons, an 18-storey mass timber building in British Colombia, Canada, was streamlined compared to similar non-timber construction. The entire timber erection portion of the construction process took only 3 months with an average crew of only 10 workers on site [1]. Additionally, the weight savings and renewable properties of timber compared to other building materials are well established. Accordingly, the use of engineered massive timber products is becoming increasingly promoted in the construction of mid- to high-rise structures. A full summary of tall massive timber buildings in the world as of June 2017 is given by CTBUH [2], in which almost 50 completed, proposed or under-construction buildings are listed. To achieve these goals of increased massive timber structures, new wood construction techniques are being rapidly developed.

Post-tensioned (PT) timber, or Pres-Lam, is a novel timber construction system which has been developed and tested over the past decade at the University of Canterbury in New Zealand. The system utilizes a technology developed originally for precast concrete to increase the potential span length and seismic performance [3]. Implementing the PT technology in timber can result in similarly improved performance, utilizing a high-strength prestressing steel tendon tightened through a cavity in a built-up timber box section. Figure 1 shows a schematic of a PT timber beam. The system improves load carrying capacity by using eccentric tendons which place the beams in a stress state of compression and negative bending preloading, so as to counteract the expected gravity load effects. Additionally, the steel anchorage and connections through multiple bays increases the seismic ductility and self-centering capacity of the structural system as a whole. In fire exposure, the cross-section of the beams and therefore the tendon eccentricity may change with charring, so a simple calculation procedure is not always available.

There has been limited development of guidance or analysis methods for PT timber systems, especially for the optimization of their design for fire performance. It is desirable to validate a numerical model for the system to increase performance-based design capability and confidence in the system, in order to expand the opportunity to adopt the system in new jurisdictions. The development and evaluation of a finite element method (FEM) model for PT timber systems is beneficial to industry as there is currently no analysis technology available to practitioners to demonstrate the system behaviour at ambient or fire conditions, and a validated FEM model is a preliminary step in understanding and developing an accessible tool for designers. A tool is necessary due to a lack of prescriptive guidance or design equations available to demonstrate compliance in many jurisdictions.

The overarching goal of this research is to facilitate the use of PT timber in Canada and abroad. This study aims to substantiate this goal by developing a methodology to model the thermo-mechanical behaviour of PT timber beams
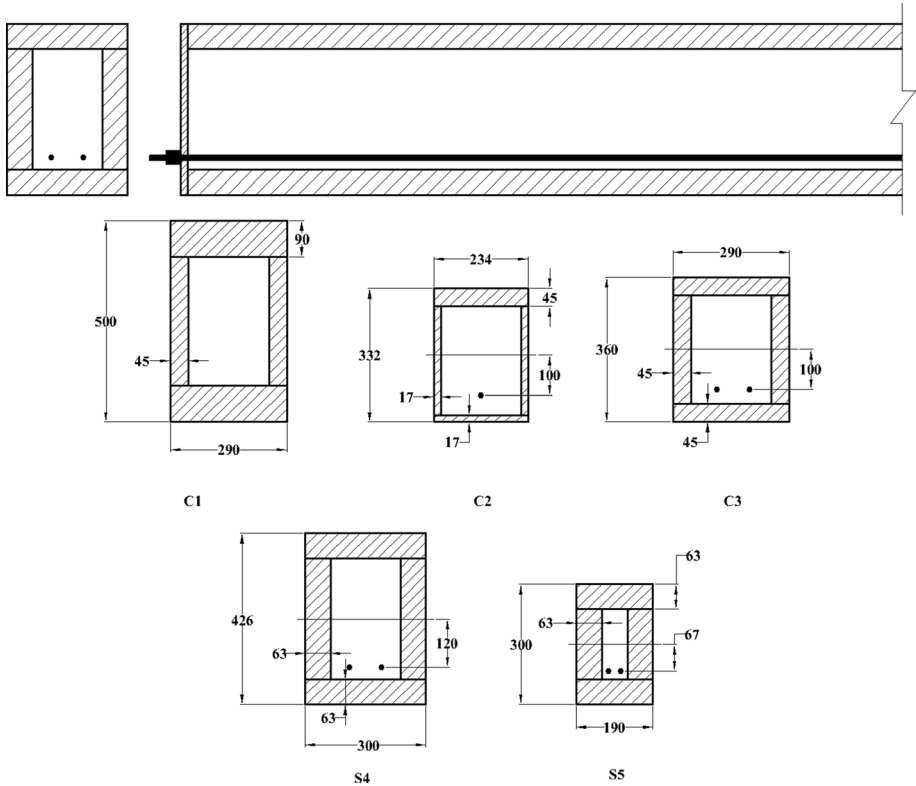
Figure 1. Schematic of a PT timber beam and cross-section dimensions of the beam tests modelled herein [4, 5].

using ABAQUS, tested against data from past representative experiments [4, 5] which are expanded upon below. ABAQUS was used as a research tool to evaluate FEM capabilities of modelling timber in fire that may be extended to a practitioner-friendly tool, utilizing accessible material definitions. It has been identified that complex or intricate models which utilize parameters and algorithms unfamiliar to the practicing engineer render the models impenetrable for their intended purpose—to advance engineering capabilities in practice [6]. A tool for use by a practicing engineer, in order to advance structural fire engineering capabilities, must be approachable and readily applied.

1.1. Experiments on PT Timber in Fire

Since the development of the PT timber system at the University of Canterbury (UC), several experiments have been done to evaluate the system performance in terms of behaviour, connections, long term effects, et cetera [4, 5, 7–10]. Two experimental studies were completed at UC on the performance of PT timber beams under fire exposure. The intent of these studies was to investigate various failure mechanisms for PT timber beams and to demonstrate whether the perfor-

mance and failure of the beams could be predicted with hand calculations. Figure 1 details the cross-sectional dimensions for the experimental beams discussed. Herein, the beam tests are referred to by the abbreviations listed in Table 1.

1.1.1. Spellman (2012) In order to investigate the performance and failure mechanisms of PT timber beams in fire, Spellman performed three large-scale standard fire furnace tests (although only two are reported in this study due to a premature failure of one of the beams—Beam B), along with several anchorage fire protection tests [4]. The timber was LVL13 and made of radiata pine, manufactured by Carter Holt Harvey in NZ [4]. The beams were loaded under four-point bending with a clear length of 4 m inside an ISO 834 standard test furnace, and a center-to-center span of 4.36 m on 100 mm-wide steel support plates [4, 11]. The two point loads were applied symmetrically with a 1.5 m spreader beam. Spellman's box-beams were built up of laminated veneer lumber (LVL) sections and were loaded at a constant level of 40 kN throughout fire exposure, approximately 49% of their ambient capacity (comparing the stress developed to their characteristic design strength). Thermal gradients were measured with thermocouples through the thickness of one web and bottom flange of the beams. The steel tendons used for post-tensioning were 7-strand wires with a nominal area of 100 mm^2 and were loaded within their elastic range [4]. Figure 1 shows the cross sections of the experimental beams.

1.1.2. Costello (2013) Spellman recommended further investigation of shear failure in PT beams after his experiments and as such, Costello's research was commissioned [5]. Costello performed several large-scale tests of timber box-beams, some with post-tensioning steel strands and some without, also shown in Fig. 1. One of the tests was completed in a furnace with an ISO 834 standard fire exposure (test C3) [11], and additional tests were completed at ambient temperature with a reduced cross-section to simulate loss of wood to charring [5]. The test specimens were also made from LVL13 of radiata pine from NelsonPine in NZ [12], and the beam span and section varied in each test. The loading schemes were all four-point bending tests with varying spreader-beam spans. In the ambient tests the load was ramped up linearly until beam failure, while in the furnace test

Table 1
Outline of Tests to be Modelled; Detailed Descriptions Provided in Sects. 1.1 and 1.2

Model	Study	Experiment description
C1	Costello [5]	Beam 3—ambient test of unmodified beam cross-section without PT tendons
C2	Costello [5]	Beam 2—ambient test of milled beam cross-section with PT tendons
C3	Costello [5]	Beam 1—furnace test with PT tendons
S4	Spellman [4]	Beam A—furnace test with PT tendons
S5	Spellman [4]	Beam C—furnace test with PT tendons

the load was held constant over the fire duration until failure. Test C1 data was used for initial model investigation as a simple ambient beam test with no post-tensioning. The beam in test C2 was milled down to a manually-reduced cross-section size to replicate the char depth from C3, and both of these tests included post-tensioning. The failure mechanisms in all of the ambient beams manifested as longitudinal shear cracks, which typically developed from the end of the beam and remained in the shear regions between the support and its adjacent loading point [5].

1.2. Numerical Modelling of Timber in Fire

There have been several past studies completed regarding the development of a material model for timber. These studies range in detail and complexity and remain a subject of debate among experts both at ambient and fire conditions. Many detailed models dissect timber at the micro-scale and use detailed material properties such as species or biological makeup, fracture characteristics, chemical processes, mass and moisture migration, et cetera. [13, 14]. Many of these properties vary considerably from product to product and involve material testing to ascertain for input into a model. A simplified set of thermal properties was developed by König [15] and later adopted in Part 1–2 of Eurocode 5, informative Annex B [16] as a method to encompass all of the changing material characteristics holistically including all of the natural processes of wood transforming to char, moisture and gas movement, and char oxidation and contraction.

In terms of mechanical properties, even at ambient conditions, a numerical model capturing the anisotropic and complex fracture mechanics of timber is difficult to produce. For simple linear structural elements, the behaviour has been represented as orthogonal and linear elastic until failure which is akin to the typical tensile failure of wood at ambient temperatures [10]. With the added complexity of temperature change affecting the wood mechanical properties, this type of definition may be no longer sufficient to capture the different failure modes of the heated timber.

Werther et al. [17] completed a study of modelling heat transfer in wood using various finite element software packages. The results using different methods of accounting for moisture evaporation were compared, including an effective specific heat method and a latent heat method. Effective specific heat values as a function of temperature are defined in Eurocode 5 Part 1–2 with a jump in the values at 100°C to account for the additional energy required to evaporate water at this temperature [16]. The latent heat method, rather, eliminates this discontinuity in the specific heat, but adds the input of a latent energy of evaporation for the total mass of water in the wood. Additionally, a mesh sensitivity study was completed. The study found that results are more stable using a latent heat method, and all software packages converged to the same results with a small enough mesh size. It was recommended that a 3 mm mesh is the optimal element size for accurate results and computational efficiency in heat transfer models.

An attempt was made by Menis to model wood in fire with an available material definition in ABAQUS, namely the Concrete Damaged Plasticity (CDP)

model [18]. It was hypothesized that this definition could be well extended to timber due to the allowance of differing strength properties for tension and compression stresses as a function of temperature. An asymmetric constitutive model is important for timber in fire due to the varying degradation in strengths with temperature. However, a drawback of the CDP model is that it may only be used with an isotropic material definition. Menis achieved agreeable results when comparing the fire performance of both CLT and LVL timber experiments using the CDP material definition.

2. Research Objectives and Approach

The objective of this study was to develop a methodology to model any type of post-tensioned timber beam. The intent was not to develop specific material properties or complex material models, but to evaluate available resources and ensure the required input parameters remain as general and accessible as possible.

PT timber has been fabricated primarily from laminated veneer lumber (LVL) in NZ. Glulam is another engineered timber product that has gained popularity for massive timber structures in Canada. The intent of this research was to investigate a general methodology that may potentially be applied to various types of wood products using different input parameters. Often LVL is modelled with three orthotropic directions: longitudinal, tangential and radial, where radial is perpendicular to the original tree growth rings and in a transverse beam axis in the final product. This is due to the manufacturing process where the veneers are cut around the logs along the growth rings and thus the radial direction is always oriented through the thickness of the veneers. Detailed wood properties typically have different values for all three of these dimensions. Glulam is manufactured in such a way that the longitudinal direction is always parallel to the wood grain, but the orientation of the laminates in the transverse directions is random. This is due to the way the laminates are cut from log cross-sections. Thus, the wood was modelled as transversely isotropic in order to maintain generality for all wood products, in which the longitudinal properties parallel to the wood grain differ from the transverse axis material properties. This accounts for the perpendicular to grain strength effects. The intent of the methodology is that it may be used with general material strength and thermal properties to vary with a range of applications.

To validate the numerical model, a series of past experiments discussed in Sect. 1.1 and outlined in Table 1 were simulated using ABAQUS finite element analysis software version 6.14. The modelling plan consisted of purely ambient mechanical analyses, thermal analyses, and fire-exposed mechanical analyses with thermal results input as predefined fields.

3. Modelling Approach

The finite element package ABAQUS/Standard was used to replicate the experiments as outlined in Table 1. ABAQUS/Standard was used as opposed to ABAQUS/Explicit to enforce equilibrium conditions for the beam tests and ensure realistic, stable results were obtained. Additionally, ABAQUS/Standard is required for heat transfer and sequentially-coupled thermal–mechanical analyses [19]. Models were first developed and validated against ambient temperature experimental results then the high-temperature effects were introduced.

3.1. Thermal Model Development

The thermal analysis is the first step in a structural fire simulation where the heating regime is applied to the structural element and a transient heat transfer analysis is completed. Heating was introduced only to the exposed surfaces of the timber beams as the steel elements were not exposed to or affected by the heat, remaining either outside the furnace or protected by the timber box-beam [4, 5]. The steel tendons remained below 100°C until failure of the furnace tests, and thus their strength remained at full capacity for the duration [20]. Additionally at 100°C, the strain from thermal expansion would be less than 0.1% using the following equation:

$$\varepsilon_t = -2.016 \times 10^{-4} + 10^{-5}T + 0.4 \times 10^{-8}T^2 \text{ for } 20°C \leq T \leq 1200°C \quad [20]$$

For wood, modelling challenges arise in relatively simple heat transfer analyses due to chemical changes in the material as it is heated to volatile combustion gases and char, and eventually to a complete loss of material around the exposed surfaces. Effective thermal properties such as those suggested in Eurocode 5, Part 1–2, Annex B, are used to capture the complex phenomena (though they are applicable only for standard fire exposures) [16]. The temperature dependent properties will change throughout the simulation at any point within the solid to represent the changes in thermal conduction, heat capacity and density due to numerous factors such as mass loss, char development and moisture migration. These suggested values as outlined in Table 2 were used in order to keep the model development generalized and not calibrated to any specific experiments.

A latent heat method was used in lieu of the jump in the effective specific heat curve recommended in the Eurocode to represent the evaporation of moisture as it offered increased stability compared to the curve discontinuity [16, 17]. The heat of evaporation of water was taken as 2260 kJ/kg [21]. The moisture content (MC) of the wood specimens tested by Costello [5] and Spellman [4] were not specified. A moisture content of 6% had been previously measured in the structural lab setting so this MC was used to estimate the MC of the PT timber beams which had been acclimatized in the lab. It is important to use the known or expected stabilized MC of the timber that is used in each specific case as it effects the thermal simulation latent heat calculation. Typical timber building moisture contents are 10% or higher which would reduce the heat transfer effects as well as the strength of the timber material. Additionally, the heat transfer model utilized is not appli-

Table 2
**Thermal Properties Defined as per Eurocode 5, Part 1–2, Annex B
[16]**

Temperature (°C)	Conductivity (W/m-C)	Density (kg/m³)	Heat capacity (J/kg-C)
20	0.12	530	1530
99		530	1770
100			13600[a]
120		500	13500[a]
121			2120
200	0.15	500	2000
250		465	1620
300		380	710
350	0.07	260	850
400		190	1000
500	0.09		
600		140	1400
800	0.35	130	1650
1200	1.5	0	1650

[a]These data points were omitted in analyses using the latent heat method

cable to realistic fires. Further testing is required to validate the modelling methodology under realistic field moisture content and fire exposure scenarios.

3.1.1. Heat Transfer Model In the initial step, a predefined field was defined for the initial ambient temperature in each analysis. A second heat transfer step was added to apply the fire exposure to the beam. The heat exposure was applied only to the three exposed surfaces of the beam as the top was protected with the furnace roof and loading apparatus. The ends of the beams which were over the supports and outside the furnace were left unexposed. The unexposed surfaces were unmodified and thus assumed to be adiabatic. The fire was reproduced from the experiments using the standard fire curve [11]. The standard fire was applied to the exposed surfaces of the beam elements as a uniform temperature field using convective and radiative heat transfer, with a film coefficient of 25 W/m²K and an emissivity of 0.8 [22]. The interior cavity surfaces also included a radiative heat transfer interaction using the cavity radiation approximation. This approximation method saves on computational requirements by using the average temperature of the cavity surface as the radiative temperature rather than calculating a view factor for each surface in the cavity to every other element. This interaction definition was tested in 2D models for comparison and was found to be a good approximation as the cavity surface generally remains isotropic throughout.

3.1.2. Mesh Refinement A mesh sensitivity study was completed on a cross-section for model C3 in order to determine the refinement required. Mesh sizes of 9 mm, 5 mm, 3 mm and 1 mm were tested, along with a combined mesh of 9 mm element sizes with smaller 3 mm thicknesses through the exposed sides. The sensitivity was evaluated at various locations on the cross-section, including the outer and

inner (cavity) surfaces at mid-height of the web and at the outer and inner nodes of a bottom corner. The available thermal data from the experiment was limited and differed from the critical areas studied herein to ensure grid independence, thus it was not compared during the mesh study. However, the refinement undertaken in this stage instilled confidence in comparisons to experimental data in other aspects discussed in Sect. 4. Figure 2 shows the convergence results for the locations aforementioned. As can be seen from Fig. 2, the 3 mm mesh results are identical to the combination mesh results in which the elements were also 3 mm through the thickness but longer perpendicular to the primary heat transfer. Comparatively, however, the combination mesh used only 30% of the computation time. The 1 mm mesh gave slightly different results for the inside surface temperatures, with a difference of about 1.5°C in the final temperature compared to the 5 mm mesh. Although the 5 mm mesh had small variances in the results from the 1 mm mesh, the 5 mm simulation took only 3% of the time compared to the 1 mm mesh. Thus, refining the mesh further increased simulation time tremendously and was not justified with the small amount of refinement in the results. Additionally, the small differences in the results only occurred either in the first few minutes of the simulation or beyond this time but well below the pyrolysis temperature. The combination mesh with 5 mm elements through the thickness was thus deemed adequate and was used for all subsequent thermal analyses.
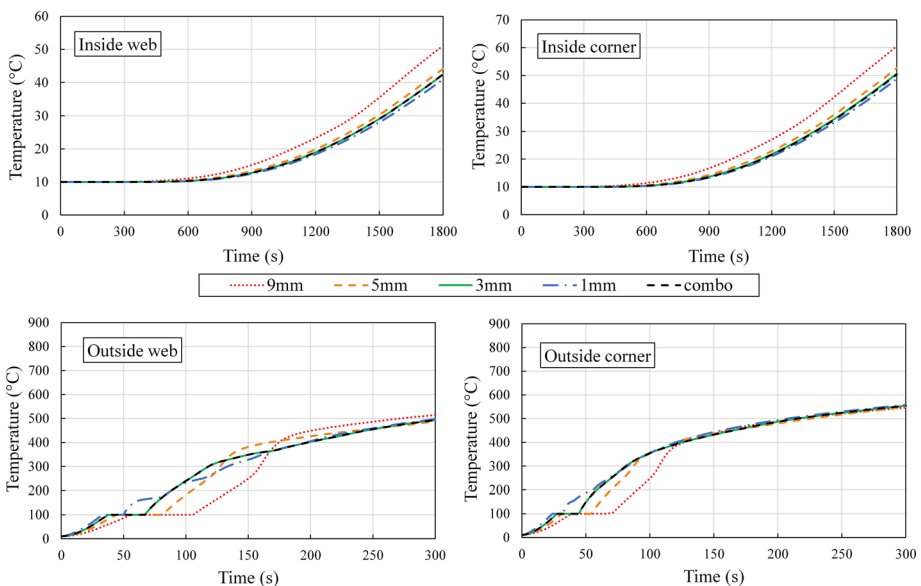

Figure 2.   Mesh refinement study for beam cross-section thermal analysis (outside node results are shown magnified to the first 300 s of the analysis as mesh sizes mostly converged after this time).

3.2. *Mechanical Model Development*

It is ideal for a finite element model to perform well for both ambient and fire conditions. The aim of this study was to first create a model that was successful at ambient conditions to ensure wood mechanical behaviour was captured, and then extend that model to a thermally dependent simulation. Figure 3 shows a graphical representation of the beam model setup. The beams were modelled with three-dimensional continuum elements (C3D8R), and the entire beams were modelled to capture any asymmetrical effects. The element type selection and mesh sensitivity study are discussed in Sect. 3.2.5. 18 mm thick steel plates were modelled with solid elements (C3D8R) as loading, support and anchorage plates where necessary. Where required, the steel PT tendons were modelled with 3D, 2-node wire beam elements (B31). The loading was modelled using steel loading plates which were tied as master surfaces to the top surface of the beam, using the surface-to-surface discretization method. The discretization method affects the formulation of the tie constraint coefficients; the surface-to-surface method is preferred for ABA-QUS/Standard and optimizes stress accuracy on the tied surfaces. This method constrains each of the nodes on the slave surface to have equal values in every degree of freedom that the nodes posses to the nearest point on the master surface.

3.2.1. *Timber Material Model* As a preliminary step, a model with isotropic elasticity was created in order to observe the effects of ignoring wood's isotropy. Although from different manufacturers, the radiata pine LVL13 products had similar characteristic design specifications from each. The manufacturers specified values for the modulus of elasticity of 13,200 MPa was used, with a typical Poisson's ratio of 0.4 [12]. This initial test was deflection controlled and resulted in behaviour which was much too stiff. This confirms that wood behaviour is highly influenced by its reduced stiffness (and strength) perpendicular to the grain. After the isotropic model produced inadequate results as expected, an orthotropic linear elastic model (using the Engineering Constants material representation) was
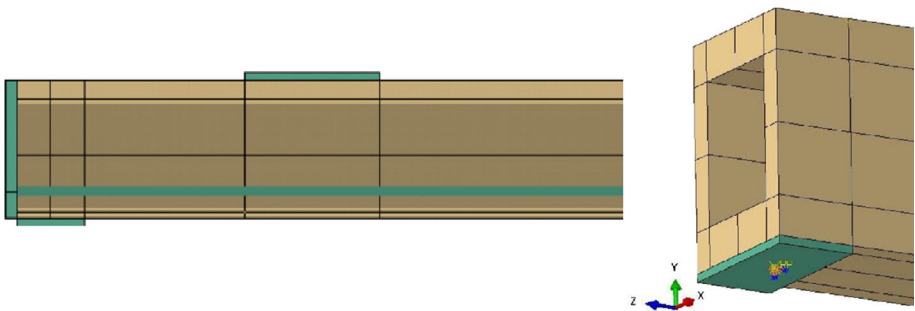

Figure 3.   Graphical representation of numerical model setup showing half of a PT timber beam with steel plates and tendon (left) and 3D view showing boundary condition (right).

defined. This allowed the material properties to be fully defined by nine constants including the three orthotropic elastic moduli, three Poisson's ratios and three shear moduli. A coordinate system was defined with the primary axis along the longitudinal beam direction, with the second axis oriented vertically (parallel to gravity) and the third axis laterally (horizontal, transverse to the axis of the beam). The values used for the engineering constants elasticity model are presented in Table 3 using manufacturer specifications for longitudinal elastic modulus and shear moduli [12]. Where material properties were not available from the manufacturer (including perpendicular to grain elastic moduli, rolling shear modulus and Poisson's ratios), average values recommended from Van Beerschoten's orthotropic model were used [10].

For the furnace test models, the engineering constants model for elasticity was employed with the moduli values dependent on temperature. The stiffness reductions with temperature given in the Eurocode 5 Part 1–2 Annex B also vary from tension to compression [16]. The reduction factor for tension was used as the compression zone of the beam is largely unaffected by temperature, due to the top flange being insulated from the heat exposure. The modification factors are specified only for the primary elastic modulus, but it was assumed that the reduction factors could also be used for the other two material directions and all the shear moduli. Table 3 gives the elastic engineering constants used as a function of temperature. ABAQUS specifies that the minimum parameter reduction allowed is 1/100th of the initial magnitude, so this requirement was used instead of the Eurocode specification of zero at 300°C [16].

To account for nonlinear effects, plasticity or damaged material behaviours were investigated. Several of such available definitions were introduced and compared to determine which could best capture the complexities of wood behaviour. ABAQUS has a number of material behaviours that were considered as candidates to represent wood nonlinear behaviour numerically. A brief introduction and the pros and cons of each type considered are listed in Table 4. Several other material model degradation and failure criteria models exist which were not considered herein but have been considered by others [23, 24]. In particular, the Hill's potential function for plasticity has been extended to criterion including asymmetric constitutive models (for example the Yamada-Sun criteria [25]) which may be

Table 3
Input Parameters for Engineering Constants Orthotropic Elasticity as a Function of Temperature

E_1 (MPa)	E_2 (MPa)	E_3 (MPa)	v_{12}	v_{13}	v_{23}	G_{12} (MPa)	G_{13} (MPa)	G_{23} (MPa)	Temperature (°C)
13,200	400	400	0.55	0.55	0.2	660	660	100	0
13,200	400	400	0.55	0.55	0.2	660	660	100	20
6600	200	200	0.55	0.55	0.2	330	330	50	100
132	4	4	0.55	0.55	0.2	6.6	6.6	1	300

Table 4
Summary of a Preliminary Comparison Between Different Model Options for Non-linear Material Modelling of Wood

Plasticity model	Pros	Cons	Notes
Concrete damage plasticity (CDP)	Asymmetrical constitutive model definition for different compressive and tensile behaviour	Requires that the elastic behaviour of the material be isotropic and linear Plasticity and damage definitions are isotropic Does not capture shear yielding	Field variables may be defined as functions of material directions, but the use of these require a user subroutine USDFLD
Plasticity with Hill's potential function	Orthotropic yield criteria	Assumes the same behaviour in tension and compression Shear strength of wood does not follow the plastic assumption $\tau = \sigma/\sqrt{3}$	The actual shear strength in each material direction may be defined as a fraction of this τ value
Fibre-reinforced composite damage	Allows for crack formulation parallel to the grain	May only be used with shell elements	Shell elements may be applicable for wood veneers or plane-type elements, however they are not ideal for general wood or heat transfer analyses
Cohesive elements	Allows for crack propagation along adhesive lines with traction versus separation for tension and shear	Will only crack along a user-defined path	Typically in tests cracks developed through the wood, not necessarily along adhesive lines
Extended finite element method (XFEM)	May use traction–separation law damage models to employ linear-elastic fracture mechanics (LEFM) No initial defect or defined crack plane is required, simply a crack nucleation criterion May be used in conjunction with orthotropic elasticity definition	Crack propagation direction cannot be defined as along the wood gin	LEFM is valid only with small-scale yielding

implemented through user subroutines in ABAQUS [23]. The intent of this research was to evaluate more simplified procedures for modelling the PT timber system.

The Hill's potential function for plasticity was able to capture wood behaviour most realistically compared to experimental observations. This material definition is compatible with an orthotropic elasticity definition such as Engineering Constants and allows for the definition of normal and shear yield strengths in each material direction. The formulation utilizes a typical anisotropic Hill's yield surface criterion associated with plastic flow through the solid elements. The constitutive model in each material direction consists of a linear elastic portion followed by a yield plateau (symmetrical in tension and compression). This is not a completely realistic constitutive model for timber and could be improved upon with an asymmetric constitutive model which captures the brittle behavior of wood in tension and softening in compression. However, with the limitations imposed on this material model, varying the constitutive model had little effect on the resulting beam behaviour. Therefore, the bilinear constitutive model is used for all simulations.

Due to the restriction of the symmetric constitutive model, a study of each model was done in order to surmise which strength properties were critical for the beam behaviour. At ambient, analyses were completed with both tensile and compressive strengths of 33 MPa and 38 MPa respectively (all parameters are summarized in the first rows of Tables 5 and 6). These values are characteristic design strengths from the manufacturer [12]. Although it is typically desirable to use a true strength value in a finite element simulation, the characteristic values were used in order to evaluate the capability of the values available to practitioners to demonstrate the behaviour of the beams conservatively. The characteristic strength values represent a worst-case scenario beam that practitioners use to design structures in reality, and are the values that would be input into a structural analysis model. These are akin to the nominal or specified design strengths referenced by manufacturers and design codes in most jurisdictions. It was observed that neither the tensile nor compressive zones reached their respective failure strengths during the ambient simulations. The compressive stresses did, however, increase above the tensile strength of 33 MPa. As such, the compressive strength was used as the tensile zones should remain linear elastic and the strength

Table 5
Characteristic Strength Values Used in Each of the Material Directions for Calculation of the Hill's Potential Function Ratios [12]

σ_0 (MPa)	f_{11} (MPa)	f_{22} (MPa)	f_{33} (MPa)	$\tau_0 = \sigma_0/\sqrt{3}$ (MPa)	f_{12} (MPa)	f_{13} (MPa)	f_{23} (MPa)	Temperature (°C)
33/38	33/38	10	10	19/22	5.3	5.3	5.3	20
21.45	21.45	2.5	2.5	12.4	2.12	2.12	1.325	100
0.33	0.33	0.1	0.1	0.191	0.053	0.053	0.053	300

Table 6
Strength Ratios Used in Hill's Potential Function for Plasticity

R_{11}	R_{22}	R_{33}	R_{12}	R_{13}	R_{23}	Temperature (°C)
1	0.303/0.263	0.303/0.263	0.278/0.242	0.278/0.242	0.278/0.242	20
1	0.117	0.117	0.171	0.171	0.107	100
1	0.303	0.303	0.278	0.278	0.278	300

would have no effect on the behaviour. A simulation applying this material to beam test C1 resulted in runaway deflections at the failure load, compared to a maximum deflection of 21.0 mm for just a purely elastic Engineering Constants model. The maximum shear stress in the shear zone between the support and the loading plate reached its limit of 5.3 MPa, compared to the experimentally measured shear stress of 6.9 MPa. This is due to the fact that the actual strength of wood is higher than the manufacturer characteristic design strength. In a design scenario, using the manufacturer strength is a conservative approach.

A summary of the temperature-dependent reduced strength values and their corresponding ratios for use in the Hill's Potential Function for plasticity for the thermal–mechanical models are shown in Tables 5 and 6. The yield strengths were those used in the ambient model modified with their temperature dependency. Another study was completed to observe the stress levels reached in the beam. This was used as the purely elastic analysis showed that the magnitude of stress within the model always remained below 33 MPa. Additionally, the compressive zone remains close to ambient temperature as the top flange is unexposed to the fire, while the tensile zone has the most heat transfer and thus reduced strength. Thus, the tensile strength of 33 MPa with the reduction factor of 0.65 from Eurocode 5 Part 1–2 Annex B [16] was used rather than the compressive strength of 38 MPa. This approach may be slightly under-conservative within the pyrolysis zones in the compression flange, as the strength would be over-predicted. For example, an element at 60°C in compression should have a strength of 23.8 MPa, however as defined herein a strength of 27.2 MPa would be computed. This was deemed acceptable as the pyrolysis zone in the compression flange affects a very small area of the cross section from which most of the load will have been redistributed, although an asymmetric model may demonstrate a more flexible behaviour. The manufacturer characteristic shear strength of 5.3 MPa was used in directions 1–2 and 1–3 with the Eurocode shear strength reduction factor of 0.4, while the same shear strength was used in the rolling shear direction with a reduction factor of 0.25 [16].

The Concrete Damaged Plasticity (CDP) definition and the XFEM damage formulation each had merits for their use as presented in Table 4, however ultimately did not perform as well as the Hill's orthotropic plasticity function. The CDP could not capture the timber box-beam stiffness due to the required isotropy and calculated a shear strength much higher than expected in wood, and so was unable to capture the shear failures seen in the experiments. As the stresses in the

beam tests did not reach their tensile or compressive strengths, no difference was observed between the CDP and purely elastic isotropic simulations. The fracture mechanics extended finite element method (XFEM) presented promising crack initiation for future investigation, however the current limitations on the defining parameters and available data on wood fracture energy limited the success of the crack propagation. Thus, the XFEM analyses resulted in similar performance to the purely elastic orthotropic simulations.

3.2.2. Steel Material Model For the steel plates and tendons, an elastic isotropic material model was employed with a Young's modulus of 200 GPa and a Poisson's ratio of 0.3 [5, 10]. In all cases, steel plates and high-strength tendons were loaded within their linear elastic range, so no material model for plasticity was required. The steel elements were all assumed to be unaffected by the heating. The thermal expansion of the tendons was negligible.

3.2.3. Mechanical Loading Phase The analysis consisted of two to four steps total (depending on experiment type). An initial step where the constraints and boundary conditions were applied, and a subsequent step where the vertical loading was applied were always defined. An intermediate step was added where the PT force was applied before vertical loading (if required). For the simulation of tests which included fire exposure, the thermal results were applied to the beam in a fourth step (after the vertical loading had been applied). The vertical load was applied linearly ramped over the step as a pressure over the surface of the two steel plates, defined by a load higher than the total force at failure in each respective experiment in order to observe the failure of each beam and at which point it would occur.

3.2.4. Boundary Conditions The model boundary conditions (BC) may significantly influence the results and require particular attention. Several different iterations of modelling these conditions were completed to investigate the effect of various scenarios and select the most realistic conditions. The support conditions were assumed to be simply supported, such that the steel support plates were pinned to allow rotation and translation on one end in the experiments except for Costello's furnace test in which the beam ends rested directly on the concrete blocks and were restrained from rotation [4, 5]. In the case of the furnace test, the steel support plates were not allowed to rotate to align with the experimental conditions that existed. The surface of the support plates were defined with a hard contact interaction with the beam bottom surface in order to ensure realistic support conditions. The span quoted in the modelled studies is assumed to be the centre-to-centre distance between supports for ambient tests and the clear span within the furnace for fire tests.

3.2.5. Mesh Refinement A study was completed on beam test C1 with 3D continuum stress elements to investigate the effects of varying element types and sizes on the model results. Model C1 was first investigated as a purely elastic, geometrically linear analysis as a preliminary step. First, the cross-section mesh size was

investigated. The thickness of the webs and flanges of this beam were 45 mm and 90 mm, respectively, and the beam span was just over 3.5 m [5]. Initially, two cross-sectional mesh sizes were compared with a constant longitudinal element size of 100 mm. The cross-section element sizes compared ranged from 5 mm to 25 mm, and the difference between the results was only 0.1%. In addition to this, the computational time of the larger cross-sectional element size was less than 1% of the time required for the smaller 5 mm cross-section elements. Thus, a cross-section mesh size of 25 mm was adequate and was used for all subsequent ambient models. It was also ensured that there were at least two elements through the thickness of webs and flanges where the elements were thinner than 50 mm.

Next, a mesh refinement study of the longitudinal mesh size was completed. A variety of element sizes were compared first for a purely elastic model as are shown in Fig. 4. The study demonstrated that there was not much difference for more coarse longitudinal mesh sizes for purely elastic analyses. There was virtually no difference between the results for the 15 mm and 25 mm longitudinal element sizes, while the 25 mm size took only 60% of the computational time compared to the 15 mm. The larger longitudinal mesh sizes also had very little difference to the 25 mm size, with the 100 mm mesh only having a difference of 0.4% less deflection.
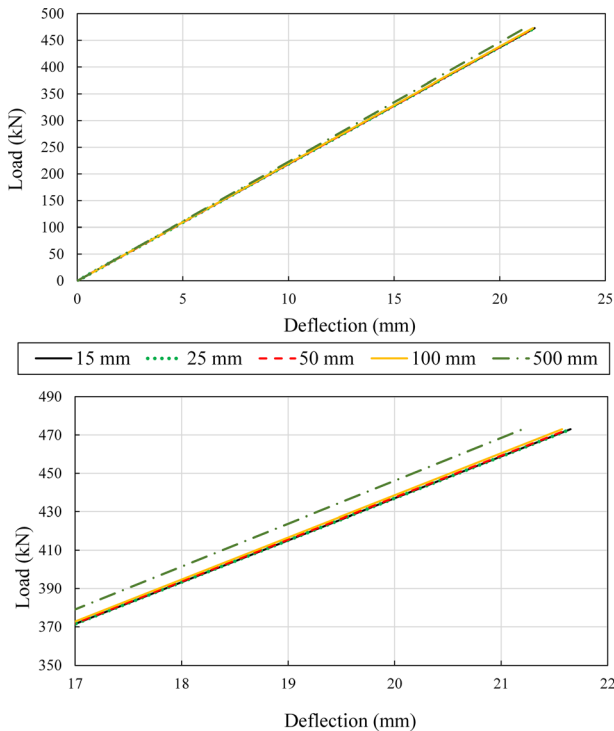

Figure 4. Longitudinal mesh refinement study of purely elastic analysis for model C1.
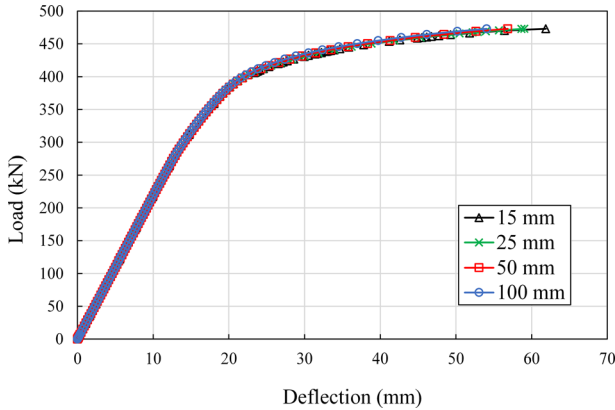
Figure 5.   Longitudinal mesh refinement study for model C1 with Hill's Potential Function for plasticity implemented.

The longitudinal mesh refinement study results with the Hill's Potential Function implemented are shown in Fig. 5. The numerical results were quite identical for all longitudinal mesh sizes considered until the end of the analysis, as the largest mesh size considered is already fairly small compared to the span length of 3 m to 4 m. Towards the end of the analysis, the smaller the element size used, the more the resulting deflection at the peak load. This is likely due to the increased flexibility from adding integration points along the length of the beam. The load–deflection curves seem to have almost reached a plateau by the peak load, however, and the amount of runaway deflections that occurred were of little consequence in reality.

A mesh sensitivity study was completed on model C3 in order to establish grid independence with thermal effects. This referred only to the elements used in the subsequent mechanical analysis, which differed from those discussed in Sect. 3.1.2 used in the thermal analysis. Three sizes of elements were compared through the 45 mm thick webs and flanges, the results of which are shown in Fig. 6. The largest mesh size consisted of 25 mm elements, but with a smaller 15 mm dimension through the web and flange thickness. A finer mesh size consisted of five elements through the web and flange thickness, thus making the nominal element dimensions in the cross-section 9 mm. The longitudinal element size in the smaller mesh was 15 mm. Finally, the medium mesh size was a hybrid between the big and small, with five elements through the web and flange thickness (9 mm dimension), but with the longer cross-sectional and longitudinal dimensions remaining at 25 mm. It can be seen in Fig. 6 that the coarse mesh results were quite different than the medium and fine mesh sizes, in which the differences were negligible. Although the results were comparatively equal for the medium and small mesh sizes, the medium mesh size required only 15% of the computation time compared to the small mesh. Thus, the medium mesh size was used for the remainder of the simulations.
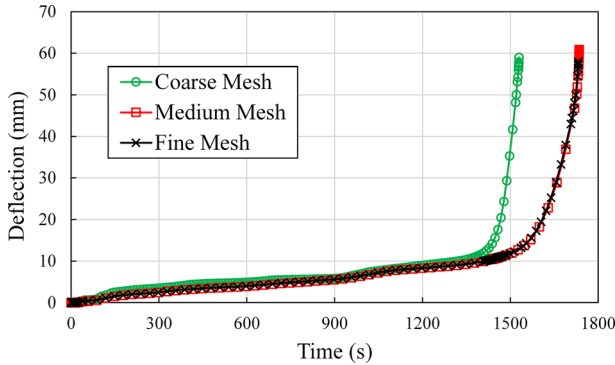
Figure 6.   Mesh sensitivity study for model C3 with three sizes of mesh elements through the 45 mm thickness: ''Coarse'' consisted of 25 mm elements (but with at least 3 elements through the thickness), ''Medium'' consisted of 25 mm elements (but with at least 5 elements through the thickness) and ''Fine'' consisted of 9 mm elements.

4. Model Validation

The numerical results for the ambient models are compared herein to the ambient experimental data (models C1 and C2) in the form of load versus deflection plots. Due to the limited success of the CDP and XFEM material models, the results were only compared for the first model (C1). A heat transfer analysis was completed for each of the furnace test experiments modelled, C3, S4 and S5. These results are compared to the available experimental data herein. Additionally, results for the sequentially coupled thermo-mechanical analyses compare the time-deflection behaviour of the beams under constant load, with the heat exposure applied from the results of the heat transfer modelling.

4.1. Ambient Test with no Post-Tensioning

Comparisons between the load–deflection behaviour of multiple simulations with varying material behaviours and the experimental results are shown for test C1 in Fig. 7. Due to the limitations discussed in Sect. 3.2.1, the CDP and XFEM results were identical to their purely-elastic counterparts. Thus, one trend is shown to represent both.

As may be observed in Fig. 7 the analyses which employed the isotropic behaviour and implemented the CDP material definition greatly underestimated the deflection of the beam. As was discussed in Sect. 3.2.1, the XFEM model results did not change from the purely elastic results (although some small cracks did initiate in appropriate locations). The orthotropic elastic definition provided agreeable results with the experimental data in terms of stiffness, with a computed elastic deflection of 86% of the experimental deflection at failure load, compared to 40% for the isotropic and CDP material definitions. The Hill's plasticity simulation followed the load–deflection behaviour until the end when the deflections

greatly exceeded the experimental values. This was due to runaway deflections which were allowed due to the lack of a fracture model, as well as experiments being halted in reality before large deformations could damage experimental equipment.

The failure mode of the beam experiment was a large crack in the shear region that extended to the center of the beam. As the Hill's plasticity definition is not able to predict crack initiation or propagation, this type of failure was not seen in the simulation. The failure began to manifest in the analysis as a shear yielding failure where the majority of the deflections occurred in the shear region. A load higher than the experimental failure load was applied so as to fail the beam in the Hill's Plasticity simulation with the results shown as the grey dashed line in Fig. 7. The failure load computed by the numerical model was 480 kN, about 1.4% larger than the actual experimental peak load of 473 kN. It was expected that the numerical model should perform worse than the experimental beam due to the use of characteristic strength, so the simulation may have significantly overestimated the failure load. This is likely due to the allowance of load redistribution through plastic elements rather than crack propagation. The numerical failure was due to runaway deflections. Such deformation was not observed in the experiment as the instrumentation was damaged following arrival at the failure load and no further deflections were recorded. Table 7 summarizes the simulation failure loads and deflections compared to experimental results.

Some tensile stresses arose perpendicular-to-grain in the vertical direction that developed around the interior corners between the top web and flanges which were much higher than the wood's perpendicular-to-grain characteristic tensile strength of around 1.4 MPa (see Fig. 8) [26]. However, in the purely elastic analyses the tensile stresses remained well below the strength limit. The increased stresses are likely due to the deformation and slight outwards buckling of the webs,
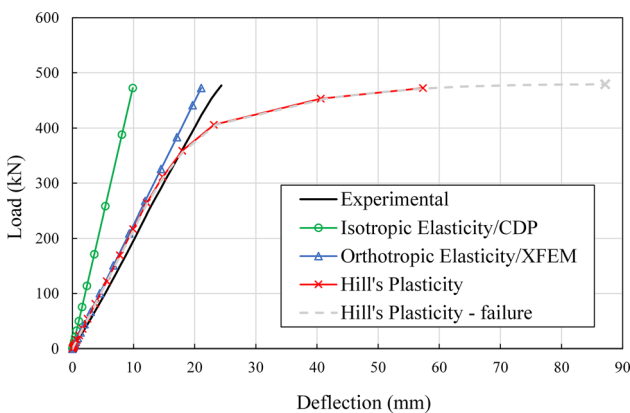

Figure 7. Comparison between C1 numerical model results and experimental data comparing multiple material models, where CDP gave identical results to Isotropic Elasticity and XFEM gave identical results to Orthotropic Elasticity [5].

Table 7
Comparison Between Numerical Model and Experimental Failure Loads and Deflections [4, 5]

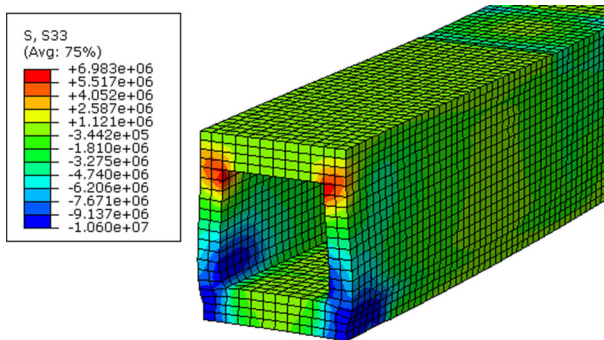| Model	Experiment failure load (kN)	Model failure load (kN)	Difference (%)	Experiment failure deflection (mm)	Model failure deflection (mm)
C1	473	480	1.5	24	87
C2	138	145	5.1	22	36

Figure 8.   Numerical model results for C1 showing stresses (in Pascal) perpendicular-to-grain in the vertical direction, with crushing around the support and excessive tensile stresses at the top flange to web connections.

due to shear yielding and crushing around the supports. This indicates that in reality a crack near the web-top flange interface would likely initiate due to the tensile stresses, similarly to the actual experiment failure mode.

4.2. Ambient Test with Post-tensioning

A comparison between the results for load–deflection behaviour of C2 to the experimental data is presented in Fig. 9. This beam test included post-tensioning. However, the results are shown with the deflections zeroed after the post-tensioning to match the presentation of the experimental data. It is observed that, unlike the other ambient simulation, the flexibility of the beam was slightly underestimated. However, the deflection was overestimated at the experiment peak load by almost 6 mm (27%).

In this simulation, the compressive stresses in both longitudinal and perpendicular-to-grain directions reached their respective yield strengths of 38 MPa and 10 MPa, showing some crushing around the supports and load plates. Additionally, both the longitudinal and perpendicular-to-grain tensile stresses did not reach their respective strength magnitudes of 33 MPa and 1.4 MPa. This demonstrates that for the model with pre-stressing, the Hill's plasticity model input assumptions using the compressive strengths were acceptable as the tensile stresses remained in the elastic range.

A failure analysis was also completed in order to observe the capability of the model to demonstrate the failure behaviour of the beam. The plasticity algorithm began to fail when the simulation was 5% above the experimental failure load. The failure mode was a shear failure in both shear regions. After this point, the software was able to converge up to 20% over the experimental peak load with several iterations. However, the deformations that occurred were unrealistic, reaching over 2 m. This was a result of the plasticity model utilized having been intended for steel in which extreme elongation is allowed, rather than a more realistic rupture which would occur in timber. If the failure point is considered as the first plasticity issue due to excessive deformation in the analysis, before the unrealistic deflections occurred, the results compared to the experimental data are shown in Fig. 9. Aside from the overestimated deflections, the behaviour shows decent agreement with the experimental data, with a failure load of 145 kN compared to the experimental peak load of 138 kN. Again, the overestimation of the failure load should be investigated further as a simulation using the characteristic strength should likely be more conservative than the actual beam performance. The results are summarized in Table 7.

4.3. Costello's Furnace Test with Post-tensioning

Costello's furnace test (C3) provided limited thermal data to compare to, as the only thermocouples located on the beam were just on the inside surface of the web and on the steel tendons. In the numerical model, it was assumed that the steel tendon would be at the temperature of the inside surface of the beam cavity. This assumption was made as the timber protects the internal tendon and the steel remains below temperatures affecting the material properties of the steel [5]. The cavity temperature experimental data compared to the numerical model results is shown in Fig. 10.

The temperatures on the internal cavity surface at the beginning and end of the simulation are quite agreeable with experimental results, however, the model tem-
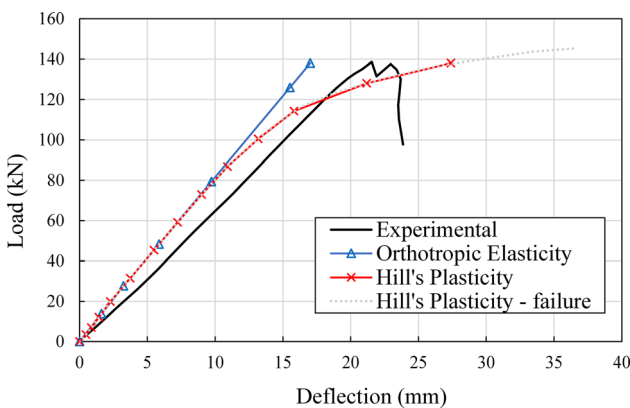

Figure 9.   Comparison between numerical results and experimental data for C2; deflections normalized after post-tensioning [5].
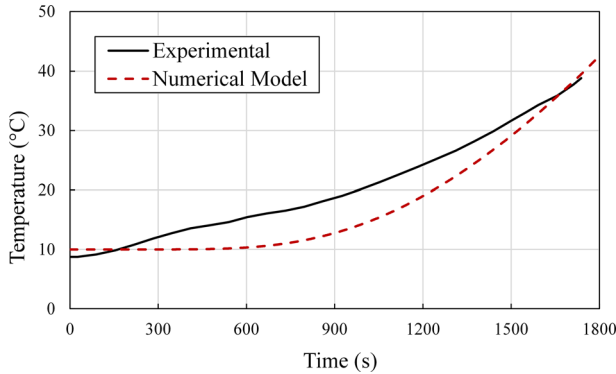
Figure 10. Comparison of C3 numerical model results for cavity temperature compared to experimental data [4].

peratures throughout the analysis are consistently lower than the experiment by about 5°C. This could be a result of some hot smoke having infiltrated into the cavity in the experiment which would have increased the temperature reading on the thermocouple. However, the discrepancies all lie in the temperature range between ambient and 40°C and thus there would be little difference in the wood material properties (less than 4%).

Costello also provided an image showing the extent of charring on a cross-section of the beam and reported 25 mm of char depth measured [5]. After 30 min of heat exposure in the numerical model, 20 mm of char was measured based on a 300°C isotherm. This is 5 mm less than the experimental char depth measured, which is quite substantial. However, in reality, the beam in the furnace would have continued to char past the recorded failure time of 29 min while the furnace was opened, the beam was removed, extinguished, and took time to cool down. This could explain the discrepancy between char depths. A comparison between the char depths at the end of the heat exposure is shown in Fig. 11 and a sum-
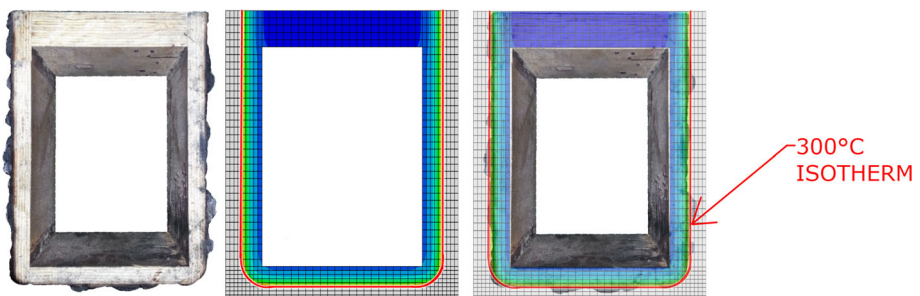

Figure 11. Comparison of C3 char depth image—modified to fix camera angle distortion from [4]—and numerical model heat transfer at 300°C maximum, with an overlay (left) and a trace (middle) of the numerical results (right).

Table 8
Comparison Between Numerical Model and Experimental Char Depths [4, 5]

Model	Experiment char depth (mm)	Model char depth (mm)	Difference (mm)
C3	25	20	− 5
S4	47.5	44	− 3.5
S5	40	39	− 1

mary of the computed char depths in each simulation compared to the experimentally observed char is shown in Table 8.

The behaviour of the beam in the numerical model for this experiment agreed quite well with the experimental results. A comparison between the mid-span deflections during the fire exposure of the model and the experiment is shown in Fig. 12. The failure time of the numerical model due to runaway deflections was 29 min, identical to the recorded experimental failure time, at which time large deflections and a loss of load occurred in the furnace [5]. This, along with the comparison between failure modes in Fig. 13, indicates that the behaviour and failure mechanism determined by the model was accurate. It is expected that if the experiment had continued and data was collected past the point where the data ends in Fig. 12, runaway deflections similar to the Hill's Potential Function simulation results would be seen.

The longitudinal compressive stresses increased slightly and reached the defined tensile strength of 33 MPa. Due to the symmetry of the constitutive model required for the Hill's formula, the compressive stresses in the model were also subject to the tensile characteristic strength limit (33 MPa) and reduction (0.65) applied. This indicates that the model may have computed some plasticity in the compressive regions before the manufacturer characteristic yield strength of 38 MPa. However, based on the Eurocode 5 Part 1–2 Annex B strength reductions, wood in compression loses its strength with temperature more dramatically than wood in tension, so this reduction in strength may have been acceptable [16].

Also, observed in Fig. 12, the CDP model does not align with the experimental behaviour of the beam. Although strengths may be input separately for compression and tension, the isotropic nature of the material model results in a stiffness that is much too high and an inaccurate shear strength calculation. The model did not nearly demonstrate the deflections or failure mechanisms seen in the experiment. It was thus concluded that the CDP model is not suitable to represent the behaviour of PT timber beams.

As discussed previously, the stress due to thermal expansion of the PT tendon was negligible compared to the PT stress. Although no tendon force data was given in Costello's furnace test results, the model tendon force remained at 107 kN for the entire simulation corresponding exactly with the PT force introduced in the experiment.
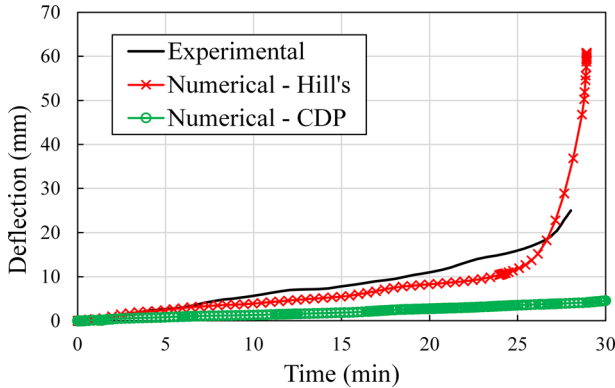
Figure 12. Vertical displacement versus time into heat exposure for C3 is shown compared to the numerical model results with both Hill's Potential Function and CDP material definitions [5].

4.4. Spellman's Furnace Tests with Post-Tensioning

Spellman's furnace tests provided substantially more recorded thermal data for comparison with the thermal numerical model results. The thermocouple placement through the thickness of the webs and bottom flanges of the furnace tests were the same, with thermocouples at 0 mm, 6 mm, 17 mm, 28 mm, 39 mm, 50 mm and 63 mm (the inside surface of the box element) [4]. Due to the slightly irregular placement of the thermocouples, the cross-section of the beam was partitioned in the model to ensure nodes were placed at the appropriate locations. This also resulted in varied mesh sizes through the thickness of those elements, with some elements slightly larger and some slightly smaller than 5 mm. The longitudinal mesh was defined the same way as described in Sect. 3.2.5.

The nodal temperatures were extracted from the analysis results at the mid-height of one web and the bottom flange, at the beam mid-span, for comparison with the experimental temperatures. A comparison of the bottom flange temperature gradient is shown for S4 in Fig. 14 and for S5 in Fig. 15.

Figure 13. Comparison of failure modes in numerical model (above) and experimental beam (below) for C3 where a shear region failure between the support outside the furnace and the load application point can be seen [5].
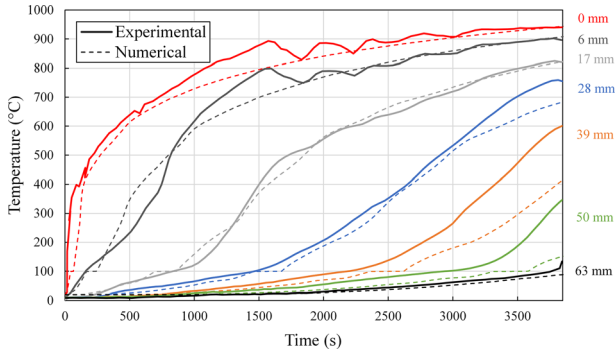
Figure 14. Bottom flange temperature distribution comparison for S4 experimental results versus numerical model [4].
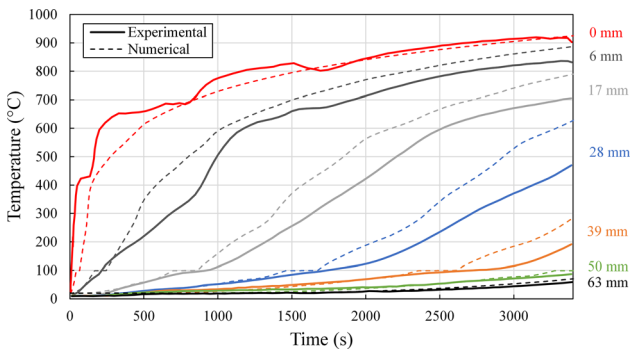

Figure 15. Bottom flange temperature distribution comparison for S5 experimental results versus numerical model [4].

As can be seen in Fig. 14, the numerical results for S4 compare quite well with the experiment. There is some discrepancy between the two results around the mid-point of the box elements, at the 39 mm and 50 mm thermocouples. The hotter temperatures recorded there in the experiment could be due to increased heat transfer from moisture migration which is not accounted for directly in the model.

Spellman did not provide an image showing char depth in his thesis, but the reported char depth after 66 min of heating was 47.5 mm [4]. The model computed a char depth of 44 mm at that time, only 3.5 mm less than measured. It is once again difficult to ascertain the direct error in these results as the amount of charring that occurred in the experimental beam after the furnace was opened was unknown, but the final char measured would most definitely be higher than that which had occurred at furnace test termination due to increased charring during cooling.

As can be seen in Fig. 15 for S5, the temperature results from the model were much higher than recorded in the experiment. However, Spellman stated in his thesis that the temperatures recorded in this experiment were abnormally low [4].

The reported char depth for this experiment after 58 min of heating was 40 mm. Despite the temperature reading discrepancies, the numerical model computed a char depth of 39 mm at this time, showing good agreement. These details indicate that an anomaly with the experimental data may have occurred, resulting in the large discrepancies between model and experiment temperature readings.

The thermal–mechanical results for Spellman's tests are also presented as deflection versus time data. In Spellman's experiments, the deflection was measured at the load actuator, and thus recorded the average displacement of the two loading points rather than the mid-span deflection. Accordingly, the deflection results from the numerical model were reported as the average vertical displacement of the central nodes on each loading plate. A comparison between the numerical and experimental results is shown in Fig. 16.

The failure time in the model for S4, due to runaway deflections, was at 66 min, two minutes later than the experimental failure time of 64 min from the same mechanism. It can be seen, however, that the failure of the beam in the simulation was much more abrupt than the more gradual failure of the experiment. The deflection remained near zero for the majority of the simulation as the PT tendon force largely counteracted the vertical load.

Much of the wood was degraded and missing from the beam once it was able to be taken out of the furnace and cooled, so it was difficult to compare the failure modes of the beams. In the deformed shape of the model beam at the end of the simulation, local buckling can be seen near the support, around where the heat exposure ended, shown in Fig. 17. Compared to the image of the beam from after the experiment, although not much can be told of the failure, some slight deformation in the same spot near the support, where the beam left the furnace, can be seen. The buckling failure in the model compared to the deflection seen in the experiment photo could be the reason that the simulation failure was much more abrupt than the experiment. Additionally, cracking was not accounted for in the model which would have caused the beam to lose stiffness, indicating that in reality the beam would have seen more deflection than in the model throughout the simulation.
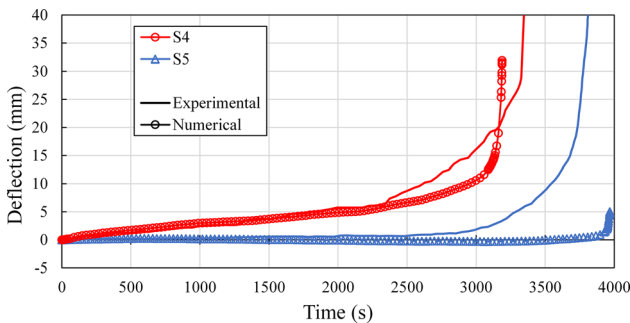

Figure 16.   Vertical displacement versus time into heat exposure for tests S4 and S5 are shown compared to the numerical model results [4].
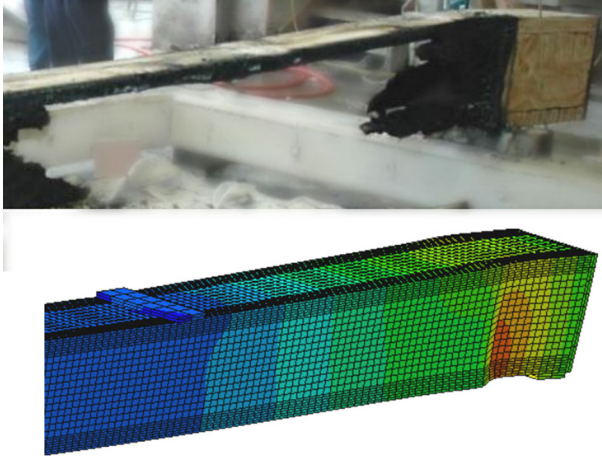
Figure 17. **Comparison between model failure mode (left) and beam after furnace test (right) for S4 where slight buckling at the furnace edge interface can be seen [4].**

Table 9
Comparison Between Numerical Model and Experimental Failure Times [4, 5]

Model	Experiment failure time (min)	Model failure time (min)	Difference (min)
C3	29	29	0
S4	64	66	+ 2
S5	56	53	− 3

A comparison between the numerical model and experimental deflections for S5 is also shown in Fig. 16. The simulation failed at 53 min due to runaway deflections, very similarly to the experimental results but three minutes earlier, as the experiment failed at 56 min. The deflections followed very accurately until around 40 min at which point, in the same way as S4, the experiment began to fail more gradually than the numerical model which had a slightly more abrupt failure. The failure mechanism in the model was due to shear and bending, while the experiment showed a clear failure due to web cracks and buckling in the shear region.

A summary of the failure time comparisons between the numerical model results and the experiments is shown in Table 9.

5. Conclusions and Recommendations

A numerical model was successfully developed and compared to post-tensioned timber beam experiments at both ambient and fire conditions using ABAQUS finite element modelling software. In general, the paper aimed to highlight the following novelties from the research study:

- The PT timber system has received a dearth of attention, particularly in the Canadian market regarding design guidance. The current capabilities and shortcomings of modelling PT timber in ambient and fire conditions using commercially available general purpose FEM software was evaluated.
- For practicing design engineers to have access to the PT timber system, an approachable and easily usable computer analysis program is required. A methodology was developed for analysing the performance of this system using a simplified formulation to demonstrate realistic behaviour.
- Through the development of this methodology, key requirements were identified for the development of a dedicated material model which is able to capture the behaviour of any timber material with readily accessible input parameters, upon further validation.
- It was illustrated that further tests on PT timber systems are required to be performed, particularly to advance the development and validation of a simplified numerical model.

As summarized in Table 7, the failure loads for the ambient beams were demonstrated reasonably well (within about 5% of the actual failure load), although the exact failure behaviour was not captured particularly well. Additionally, the failure loads should be conservatively underestimated with the use of the characteristic design strength in the simulations. These shortcomings could be improved upon with a more intricate timber failure criterion that includes the brittle behaviour of timber in tension and shear, and crack propagation. On the other hand, the heat transfer models showed good results when compared with the available experimental data. The importance of having an accurate estimate of material density and moisture content was apparent. The computed char depths were always slightly smaller than the measured char which could be due to additional charring in the cooling or extinction phases of the furnace tests which are not accounted for in the model. The study indicated that a model which includes the orthotropic nature of wood in the material definition is more significant to the behaviour results than the need to differentiate between tensile and compressive strengths. However, for the most realistic and reliable results, a model where both phenomena may be captured simultaneously is desired. Finally, the thermo-mechanical model results for all scenarios showed impressive accuracy when compared to the experimental data. The Hill's Potential Function for the plasticity behaviour of wood proved to be much more suited to this modelling scenario than others, including the Concrete Damaged Plasticity and XFEM material behaviours. Typically, the numerical model followed the deflection behavior of the experiment quite well. The model failure modes were comparable but were typi-

cally more abrupt than the experiment, with the failure times always within a few minutes of the actual experiment times. Due to the deflections governing the failure of these beams, the strength used had less of an impact on the results. It is recommended that the modelling methodology presented herein be further validated against another set of PT timber beam tests, with particular care against the conservatism of the model for design purposes using the characteristic strength values.

This study highlighted many shortcomings of the readily available material formulations in ABAQUS and thus identified important aspects of material definitions that should be included in a complex timber model. More development is required in order to implement these aspects as there is not an available material definition which includes them all that is readily accessible to practitioners. For a methodology or tool readily accessible to practitioners for exploratory or design purposes, it should be usable without complex coding or sophisticated knowledge of FEM, or intricate material properties which may be obtained only from lab testing. Currently the only method of employing more accurate timber models to the knowledge of the authors is through the use of user subroutines while using general purpose commercial FEM software. The authors stress once again that the future development of this methodology must address the shortcomings of the previously available material formulations and be validated with further testing. From the findings of this study and with more development and validation, an FEM formulation which captures the heat transfer, material stiffness and failure criteria properties of timber for use by practitioners may be on the horizon, and will provide increased opportunities for the design and use of this advanced timber structural system.

Acknowledgements

References

1. Pilon A et al (2017) Brock commons Tallwood house: construction overview. University of British Columbia's Centre for interactive research on sustainability, Naturally: Wood, BC. http://wood-works.ca/wp-content/uploads/brock_commons_-_construction_overview.pdf
2. CTBUH (Council on Tall Buildings and Urban Habitat) (2017) Tall timber: a global audit, in tall buildings in numbers. CTBUH J, (II)47–49. http://global.ctbuh.org/resources/papers/3350-TBIN.pdf
3. Palermo A, Pampanin S, Buchanan A, Newcombe M (2005) Seismic design of multi-storey buildings using Laminated Veneer Lumber (LVL). In: Proceedings of the New Zealand society for earthquake engineering conference, paper 14
4. Spellman PM (2012) The fire performance of post-tensioned timber beams. University of Canterbury, Christchurch

5. Costello RS (2013) The fire performance of post-tensioned timber buildings. University of Canterbury, Christchurch
6. Law A (2016) The role of modelling in structural fire engineering design. Fire Saf J 80:89–94. https://doi.org/10.1016/j.firesaf.2015.11.013
7. Buchanan A, Palermo A, Carradine DM, Pampanin S (2011) Post-tensioned timber frame buildings. Struct Eng 89(17):24–30
8. Granello G, Leyder C, Frangi A, Palermo A, Chatzi E (2019) Long-term performance assessment of an operative post-tensioned timber frame structure. J Struct Eng 145(5):04019034
9. Wanninger F, Frangi A (2014) Experimental and analytical analysis of a post-tensioned timber connection under gravity loads. Eng Struct 70:117–129. https://doi.org/10.1016/j.engstruct.2014.03.042
10. Van Beerschoten WA (2013) Structural performance of post-tensioned timber frames under gravity loading. University of Canterbury, Christchurch
11. ISO (International Organization for Standardization) (2014) ISO 834-10. fire resistance tests: elements of building construction. International Organization for Standardization, Geneva
12. Nelson Pine Industries Limited (2016) Laminated veneer lumber: specific engineering design guide. http://www.nelsonpine.co.nz/wp-content/uploads/LVL_Specific_Engineering_Design_Guide.pdf
13. Fredlund B (1993) Modelling of heat and mass transfer in wood structures during fire. Fire Saf J 20:39–69
14. Richter F, Rein G (2018) The role of chemistry in predicting the charring rates under realistic fire conditions. In: 12th international performance-based codes and fire safety design methods, Honolulu, USA
15. König J (2005) Structural fire design according to Eurocode 5—design rules and their background. Fire Mater 29:147–163. https://doi.org/10.1002/fam.873
16. CEN (European Committee for Standardization) (2004) Annex B: (informative) advanced calculation methods, part 1–2: general—structural fire design, Eurocode 5: design of timber structures. British Standards Institute, London, pp. 20–28
17. Werther N, O'Neill JW, Spellman PM, Abu AK, Moss PJ, Buchanan AH, Winter S (2012) Parametric study of modelling structural timber in fire with different software packages. In: Proceedings of the 7th international conference on structures in fire, pp 427–436
18. Menis A (2012) Fire resistance of Laminated Veneer Lumber (LVL) and Cross-Laminated Timber (XLAM) elements. Università Degli Studi di Cagliari, Cagliari
19. Dassault Systèmes (2012) Section 27.1.1 element library: overview in ABAQUS analysis user's guide, ABAQUS 6.14. Dassault Systèmes Simulia Corp., Providence, RI
20. CEN (European Committee for Standardization) (2004) Section 3.4: thermal elongation of reinforcing and prestressing steel, part 1–2: general rules—structural fire design, Eurocode 2: design of concrete structures. British Standards Institute, London, pp. 28–29
21. Drysdale DD (2016) Heats of combustion, Section 5—thermochemistry. In: Hurley MJ (ed), SFPE handbook of fire protection 5th edition. Society of Fire Protection Engineers, Springer, Berlin, pp 138–150. https://doi.org/10.1007/978-1-4939-2565-0_5
22. CEN (European Committee for Standardization) (2004) Section 3 thermal actions for temperature analysis, part 1–2: general rules—actions on structures exposed to fire, Eurocode 1: actions on structures. British Standards Institute, London, pp. 23–24
23. Chen Z, Zhu E, Pan J (2011) Numerical simulation of mechanical behaviour of wood under complex stress. Chin J Comput Mech 28(4):629–634 + 640

24. Zhang J, Wang Y, Li L, Xu Q (2017) Thermo-mechanical behaviour of dovetail timber joints under fire exposure. Fire Saf J . https://doi.org/10.1016/j.firesaf.2017.11.008
25. Yamada S, Sun C (1978) Analysis of laminate strength and its distribution. J Compos Mater 12(3):275–284. https://doi.org/10.1177/002199837801200305
26. Ardalany M, Deam B, Fragiacomo M, Crews KI (2011) Tension perpendicular to grain strength of wood, Laminated Veneer Lumber (LVL), and cross-banded LVL (LVL-C). In: Proceedings of the 21st Australasian conference on the mechanics of structures and materials, pp 891–896